Chapter 17

Finite Volume Method

. This chapter focusses on introducing finite volume method for the solution of partial differential equations. These methods have gained wide-spread acceptance in recent years for their robustness, their intuitive formulation, and their computational advantages. We will take the opportunity to look at issues pertaining to method formulation, discretization, and analysis.

17.1 The partial differential equation

The partial differential equation we will focus on is a scalar equation that represents the transport of a substance under the influence of advection by the air flow and mixing. The transport equation is frequently written in the **advective** form:

$$\frac{\partial T}{\partial t} + \vec{u} \cdot \nabla T = \nabla \cdot (\alpha \nabla T) \tag{17.1}$$

where T is the subtance transported, e.g. temperature, humidity or a pollutant concentration, $\vec{u}$ is the velocity field presumed known, and α is the diffusion coefficient and which can represent either molecular diffusion or eddy mixing.

The velocity field cannot be arbitrary and must satisfy some sort of mass conservation equation. Here we will assume the flow to be incompressible so that its mass conservation equation reduces to:

$$\nabla \cdot \vec{u} = 0 \tag{17.2}$$

The advective form can be interpreted as the time evolution of the T field along characteristic lines given by $\frac{\mathrm{d}x}{\mathrm{d}t} = \vec{u}$. It is thus closest to a Lagrangian description of the flow where one follows individual particles. In the Eulerian frame, however, another important issues is the conservation of the tracer T for long period of times. This stems not only from physical considerations but also for the need to account for the sources and sinks of T in long calculations. It

is imperative that the discretization does not introduce spurios sources (this the prime imperative in climate models for example). A slightly different form of the equation called the **conservative** form can be derived and forms the starting point for the derivation of finite volume methods. Multiplying the continuity equation by T, adding it to the resultant equations to the advective form, and recalling that $\vec{u} \cdot \nabla T + T \nabla \cdot \vec{u} = \nabla \cdot (\vec{u} T)$ we can derive the conservative form of the transport-diffusion equation:

$$\frac{\partial T}{\partial t} + \nabla \cdot (\vec{u} T) = \nabla \cdot (\alpha \nabla T). \tag{17.3}$$

17.2 Integral Form of Conservation Law

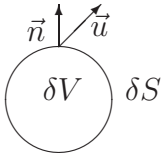

Figure 17.1: Skectch of the volume δV and its bounding surface δS.

The partial differential equation is valid at all **points** in the domain which we could consider as infitesimal volumes. Anticipating that infinitesimal discrete volumes are unaffordable and would have to be "inflated" to a finite size, we proceed to derive the conservative form for a finite volume δV bounded by a surface δS as shown in figure 17.1; the integral yields:

$$\int_{\delta V} \frac{\partial T}{\partial t} \, \mathrm{d}V + \int_{\delta V} \nabla \cdot (\vec{u} T) \, \mathrm{d}V = \int_{\delta V} \nabla \cdot (\alpha \nabla T) \, \mathrm{d}V \tag{17.4}$$

$$\frac{\mathrm{d}}{\mathrm{d}t} \left(\int_{\delta V} T \, \mathrm{d}V \right) + \int_{\delta S} \vec{n} \cdot \vec{u} T \, \mathrm{d}V = \int_{\delta S} \vec{n} \cdot \alpha \nabla T \, \mathrm{d}V \tag{17.5}$$

Remarks

- We assume the volume δV to be fixed in space so we can interchange the order of integration in space and differentiation in time. The interpretation of the first integral on the left hand side of equation 17.5 is now simple: it is the time rate of change of the T budget inside volume δV.

- We have used the Gauss-divergence theorem to change the volume integrals of the flux and diffusion divergence into surface integrals. Here $\vec{n}$ is the outward unit normal to the surface δS. The surface integral on the left hand side accounts for the advective flux carrying T in and out of the volume δV across the surface δS; the one on the right hand side accounts for the diffusive transport of T across δS.

- Equation 17.5 lends itself to simple physical interpretation: the rate of change of the T budget in δV is equal to the rate of transport of T through δS by advective fluxes (transport by the flow, wind, current) and diffusive fluxes.
- If the volume δV is closed to advection or diffusion: $\vec{u}.\vec{n} = 0$ and $\nabla T \cdot \vec{n} = 0$, then the rate of change is zero and the budget of T is conserved within δV.
- The volume δS is so far arbitrary and we have not assigned it a specific shape or size. Actually equation 17.5 applies to any volume δV whether it is a computational cell, an entire ocean basin, or Earth's atmosphere.
- If there are additional physical processes affecting the budget of T, such as sources or sinks within δV these should be accounted for also. No additional process is considered here.
- The derivatives appearing in the diffential equation 17.1 are: first order for the advective term, and second order for the diffusion term, whereas the equivalent terms in the integral form have only a zero-th order derivative and first order derivative respectively. This lowering of the derivative order is important in dealing with solution which change so rapidly in space that the spatial derivative does not exist. Examples include supersonic shock waves in the atmosphere or hydraulic jump in water where fluid properties such as density or temperature change so fast that it appears **discontinuous**. Discontinuous function do not have derivatives at the location of discontinuity and mathematically speaking the *partial differential* form of the conservation equation is invalid there even though the conservation law underlying it is still valid. Special treatment is generally required for treating discontinuities and reducing order of the spatial derivative helps simplify the special treatment. For these reasons Finite volumes are preferred over finite differences to solve problems whose solution exhibit local discontinuities.

A slightly different form of equation 17.5 can be derived by introducing the average of T in δV and which we refer to as $\overline{T}$ and is defined as:

$$\overline{T} = \frac{1}{\delta V} \int_{\delta V} T \, \mathrm{d}V. \tag{17.6}$$

The integral conservation law can now be recast as a time evolution equation for $\overline{T}$:

$$\delta V \frac{\mathrm{d}\overline{T}}{\mathrm{d}t} + \int_{\delta S} \vec{n} \cdot \vec{u} T \, \mathrm{d}V = \int_{\delta S} \vec{n} \cdot \alpha \nabla T \, \mathrm{d}V \tag{17.7}$$

17.3 Sketch of Finite Volume Methods

Equation 17.5 and 17.7 are exact and no approximation was necessary in their derivation. In a numerical model, the approximation will be introduced by the

temporal integration of the equations, and the need to calculate the fluxes in space and time. The traditional finite volume method takes equation 17.7 as its starting point. The domain is first divided into **computational cells** δV_j where the cell average of the function is known. The advection and diffusion fluxes are calculated in two steps:

- **Function reconstruction** The advective fluxes require the calculation of the function values at cell edges, while the diffusive fluxes require the calculation of the function derivative at cell edges. The latter are obtained from approximating the function T with a polynomial whose coefficients are determined by the need to recover the cell averages over a number of cells.

$$\tilde{T} = \sum_{n=1}^{P} a_n \phi(\mathbf{x}) \tag{17.8}$$

$$\int_{\delta V_{j+m}} \tilde{T} \, \mathrm{d}V = \delta V_{j+m} \overline{T}_{j+m}, \quad m = 0, 1, 2, \ldots, P-1 \tag{17.9}$$

  where δV_{j+m} are P cells surrounding the cell δV_j and where the ϕ_n are P suitably chosen interpolation functions (generally simple polynomials). The unknown coefficients a_n are recovered simply from the simultaneous algebraic equation

$$\sum_{n=1}^{P} A_{m,n} a_n = \delta V_{j+m} \overline{T}_{j+m}, \quad A_{m,n} = \int_{\delta V_{j+m}} \phi_n \, \mathrm{d}V. \tag{17.10}$$

  Once the coefficients a_n are known it becomes possible to evaluate the function on cell edges with a view to compute the flux integrals. The error in the spatial approximation is primarily due to equation 17.8.

- **Evaluation of the integrals.** The integrals are usually evaluated numerically using Gauss type quadrature. The approximation function ϕ_n generally determine the number of quadrature points so that the quadrature is exact for polynomials of degree P. No error is then incurred during the spatial integration. One can then write:

$$F_j = \sum_{q=1}^{Q} \left[\vec{u} \cdot \vec{n} \tilde{T} |\delta S_j| \right]_{\vec{x}_q} \omega_k \tag{17.11}$$

  where ω_k are the weights of the Gaussian quadrature (as appropriate for multi-dimensional integration, $\vec{x}_q$ are the Q quadrature points, and δS_j are the mapping factors of the surface δS_j

- **Temporal integration** The final source of error originates from the temporal integration whereby the fluxes are used to advance the solution in time

using a time marching procedure a la Forward Euler, one of the Runge Kutta methods, or the Adams-Bashforth class of methods. The time integration cannot be chosen independtly of the spatial approximation, but is usually constrained by stability considerations.

17.4 Finite Volume in 1D

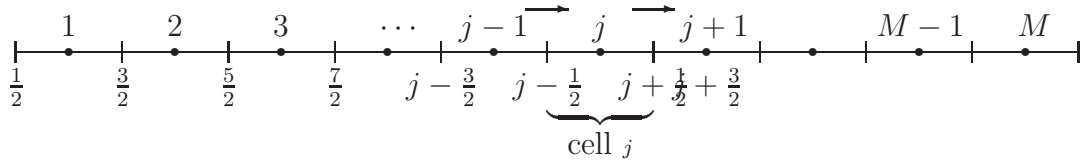

Figure 17.2: Discretization of a one-dimensional domain into computational cells of width δx. The cell centers are indicated by filled circles and cell edges by vertical lines |; the *cell number* is shown above the cells while the numbers below the line indicate cell edges.

To illusrate the application of the procedure outlined in the previous section it is best to consider the simple case of one-space dimension. In that case the cells are line segments as shown in figure 17.2. The cell volumes reduces to the width of the segment δx which we assume to be the same for all cells in the following. The flux integrals reduce to evaluation of the term at the cell edges. The conservation law can now be written as:

$$\frac{\mathrm{d}\overline{T}_j}{\mathrm{d}t} = -\frac{F_{j+\frac{1}{2}} - F_{j-\frac{1}{2}}}{\delta x} + \frac{D_{j+\frac{1}{2}} - D_{j-\frac{1}{2}}}{\delta x} \tag{17.12}$$

where $F_{j+\frac{1}{2}} = uT$ and $D_{j+\frac{1}{2}} = \alpha T_x$ are the advective flux and diffusive fluxes at $x_{j+\frac{1}{2}}$.

17.4.1 Function Reconstruction

The function reconstruction procedures can be developed as follows prior to time-integration. Assume

$$T = \sum_{n=0}^{P} a_n \xi^n, \text{ where } \xi = \left(\frac{x - x_j}{\delta x_j}\right) \tag{17.13}$$

Here a_n are the $P+1$ coefficients that need to be determined from $P+1$ conditions on the averages of the polynomials over multiple cells. The origin and scale of the coordinate system have been shifted to the centre of cell j and scaled by its width

for convenience so that the left and right edges are located at a scaled length of -1/2 and 1/2, respectively. The entries of the matrix are now easy to fill since

$$A_{m,n} = \int_{x_{m-\frac{1}{2}}}^{x_{m+\frac{1}{2}}} \left(\frac{x - x_{j-\frac{1}{2}}}{\delta x_j} \right)^{n-1} \mathrm{d}x, \quad \text{for } n = 1, 2, \ldots, P+1 \tag{17.14}$$

$$= \frac{\delta x_j}{n} \left[\left(\frac{x_{m+\frac{1}{2}} - x_{j-\frac{1}{2}}}{\delta x_j} \right)^n - \left(\frac{x_{m-\frac{1}{2}} - x_{j-\frac{1}{2}}}{\delta x_j} \right)^n \right] \tag{17.15}$$

$$= \delta x_j \frac{\xi^n_{m+\frac{1}{2}} - \xi^n_{m-\frac{1}{2}}}{n}, \text{ with } \xi_{m\pm\frac{1}{2}} = \frac{x_{m\pm\frac{1}{2}} - x_j}{\delta x_j} \tag{17.16}$$

17.4.2 Piecewise constant

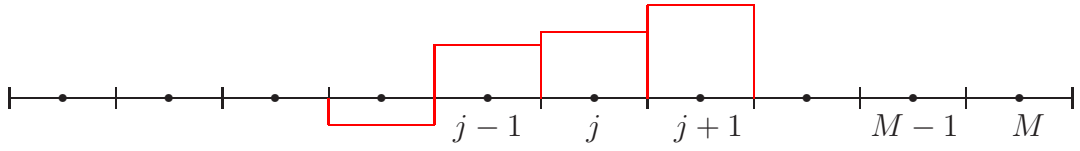

Figure 17.3: Piecewise constant approximation.

The simplest case to consider is one where the function is constant over a cell as shown in figure 17.3. Then we have the approximation:

$$T = a_0 \tag{17.17}$$

Since there is only one unknown coefficient, a_0, we can only impose a single constraint, namely that the integral of T over cell j yields $\delta x_j \overline{T}_j$:

$$\int_{x_{j-\frac{1}{2}}}^{x_{j+\frac{1}{2}}} a_0 \, \mathrm{d}x = \delta x_j \overline{T}_j \tag{17.18}$$

The solution is then simply $a_0 = \overline{T}_j$. The function reconstruction at $x_{j+\frac{1}{2}}$ can be done. There are a couple of things to notice first with respect to implementing the solution algorithm:

- The edge point two approximations are possible, one from the left cell j and one from the right cell $j+1$. For the purpose of defining the advective flux, a physically intuitive justification is that the information reaching the edge should come from the **upstream** cell, i.e. the cell where the wind is blowing from. Thus we have:

$$T_{j+\frac{1}{2}} = \begin{cases} \overline{T}_j & \text{if } u_{j+\frac{1}{2}} \geq 0 \\ \overline{T}_{j+1} & \text{if } u_{j+\frac{1}{2}} < 0 \end{cases} \tag{17.19}$$

- Piecewise constant function have a zero spatial derivative, and hence piecewise constants are useless for computing the function derivation for the diffusion term.

17.4.3 Piecewise Linear

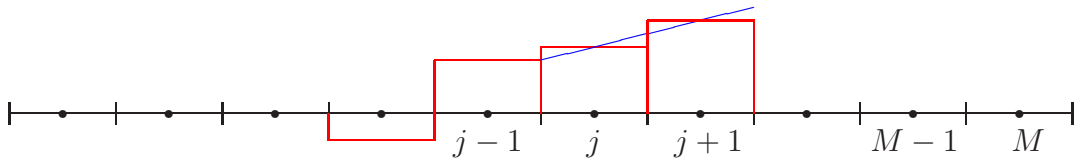

Figure 17.4: Piecewise Linear Approximation.

An improvement over the constant approximation is to assume linear variations for the function over two cells as shown in figure 17.4. Then we have the approximation:

$$T = a_0 + a_1 \xi \tag{17.20}$$

Since there are two unknown coefficient, a_0 and a_1, we need to impose two integral constraints. The choice of **reconstruction stencil** is at our disposal; here we choose a symmetric stencil consisting of cells j and $j+1$ so that $x_{j-\frac{1}{2}} \leq x \leq x_{j+\frac{3}{2}}$; equivalently $-\frac{1}{2} \leq \xi \leq \frac{3}{2}$. The two constraints become:

$$\int_{-\frac{1}{2}}^{\frac{1}{2}} a_0 + a_1 \xi \, \mathrm{d}\xi = \overline{T}_j \tag{17.21}$$

$$\int_{\frac{1}{2}}^{\frac{3}{2}} a_0 + a_1 \xi \, \mathrm{d}\xi = \frac{\delta x_{j+1}}{\delta x_j} \overline{T}_{j+1} \tag{17.22}$$

Performing the integration we obtain the following system of equations for the unknowns:

$$\begin{pmatrix} 1 & 0 \\ 1 & 1 \end{pmatrix} \begin{pmatrix} a_0 \\ a_1 \end{pmatrix} = \begin{pmatrix} \overline{T}_j \\ \dfrac{\delta x_{j+1}}{\delta x_j} \overline{T}_{j+1} \end{pmatrix} \tag{17.23}$$

When the grid cells are of constant size the solution is simply:

$$a_0 = \overline{T}_j, a_1 = \overline{T}_{j+1} - \overline{T}_{j-1} \tag{17.24}$$

The linear interpolation is then

$$T = \overline{T}_j + \left(\overline{T}_{j+1} - \overline{T}_j\right) \xi \tag{17.25}$$

$$= (1-\xi)\overline{T}_j + \xi \overline{T}_{j+1}, \text{ for } -\frac{1}{2} \leq \xi \leq \frac{3}{2} \tag{17.26}$$

To evaluate the function at the cell edge $\xi_{j\pm\frac{1}{2}}$ it is enough to set $\xi = \pm\frac{1}{2}$.

17.4.4 Piecewise parabolic

For parabolic interpolation centered on the cells $j-1$, j and $j+1$, the polynomial takes the form

$$T = \left[\frac{-\overline{T}_{j+1} + 26\overline{T}_j - \overline{T}_{j-1}}{24}\right] + \left[\frac{\overline{T}_{j+1} - \overline{T}_{j-1}}{2}\right]\xi + \left[\frac{\overline{T}_{j+1} - 2\overline{T}_j + \overline{T}_{j-1}}{2}\right]\xi^2$$
$$\text{for } -\frac{3}{2} \leq \xi \leq \frac{3}{2}, \xi = \frac{x - x_j}{\delta x} \tag{17.27}$$

At $x_{j+\frac{1}{2}}$ the cell edge value can now be computed by setting $\xi = 1/2$ in the expression above to get:

$$T_{j+\frac{1}{2}} = \frac{-\overline{T}_{j-1} + 5\overline{T}_j + 2\overline{T}_{j+1}}{6} \tag{17.28}$$

17.4.5 Reconstruction Validation

The validation of the characteristics of the different reconstruction procedures will be illustrated here by looking at some important examples. In order to characterize the procedures accurately, we need to solve a problem with a known solution, and compare the results to what the numerical scheme yields. The result is of course the error in the reconstruction. We will look at several examples with distinct characteristics: function with smooth variations, and functions with local kinks in the graphs. The kinks are symptomatic of a break in the smoothness of the function, as in when the slope of the graph changes abruptly (slope discontinuity) or when the value of the function itself changes abruptly (function discontinuity). In all cases we will be interested in monitoring the decrease of the error with increasing number of cells (decreasing δx) for different functions, and for each of the reconstruction procedures.

Infinitely smooth profile

Our first example consists of reconstructing the function $T = \cos \pi x$ on the interval $-1 \leq x \leq 1$, starting from its analytical cell average over cell j:

$$\overline{T}_j = \frac{1}{\delta x}\int_{x_{j-\frac{1}{2}}}^{x_{j+\frac{1}{2}}} \cos \pi x \, \mathrm{d}x = \frac{\sin \pi x_{j+\frac{1}{2}} - \sin \pi x_{j-\frac{1}{2}}}{\pi \delta x} \tag{17.29}$$

The result of the reconstruction using the piecewise constant, linear and parabolic reconstruction are shown by the symbols in figures 17.5-17.7, respectively, and the error at each cell edge is given by the height difference between the solid curve (reference solution) and the symbol.

Remarks

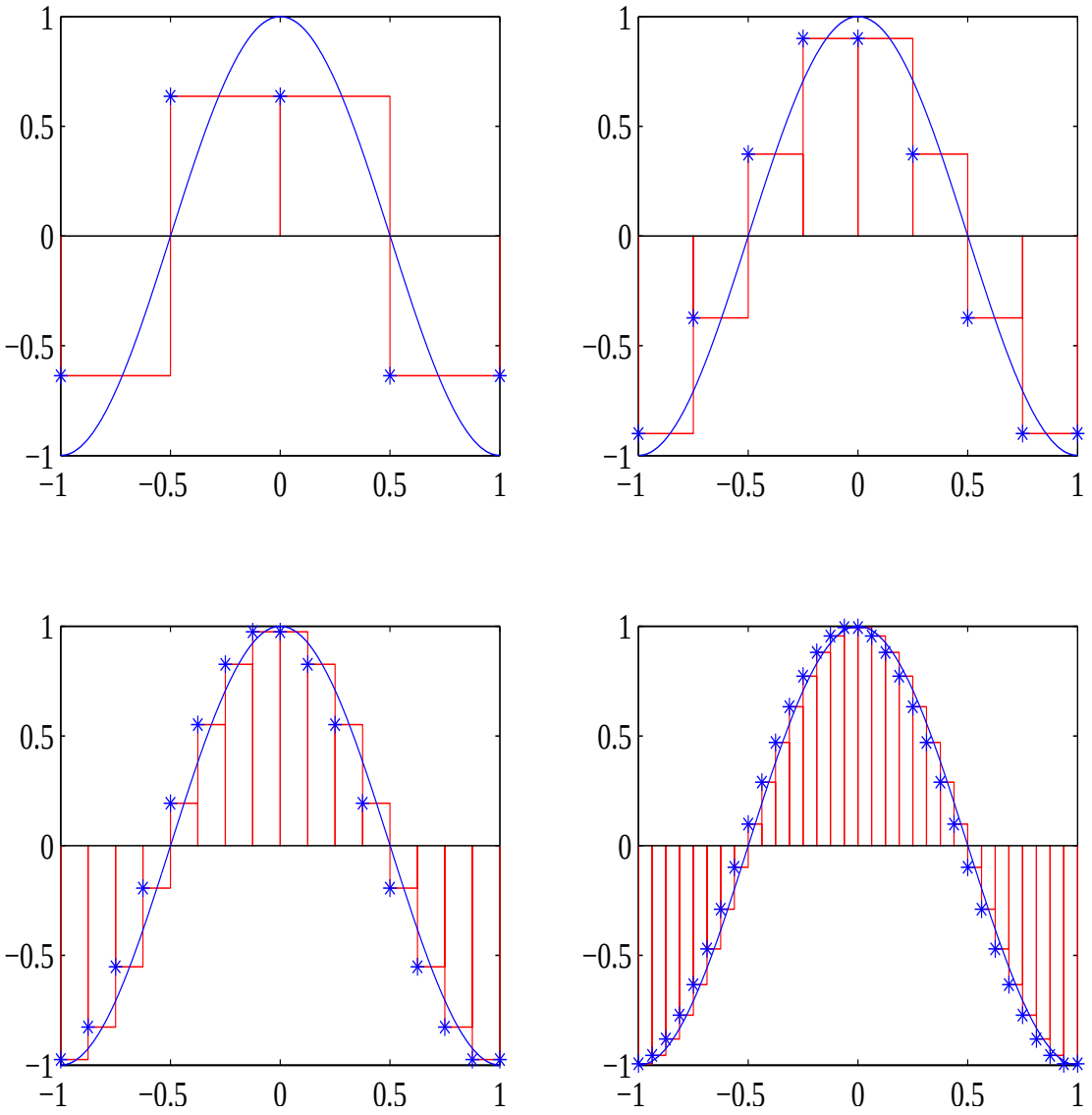

Figure 17.5: Reconstruction at cell edges using piecewise constant reconstruction with 4 (top left), 8 (top right), 16 (bottom left) and 32 (bottom right) cells. The solid curved line is the exact solution, whereas the staircases represent the cells and the cell averages. In the present case we have assumed that the wind is blowing from left to right except at the right most cell. The * symbols are the values of T calculated by the reconstruction procedure. The error is thus the height difference between the solid curve and the symbols.

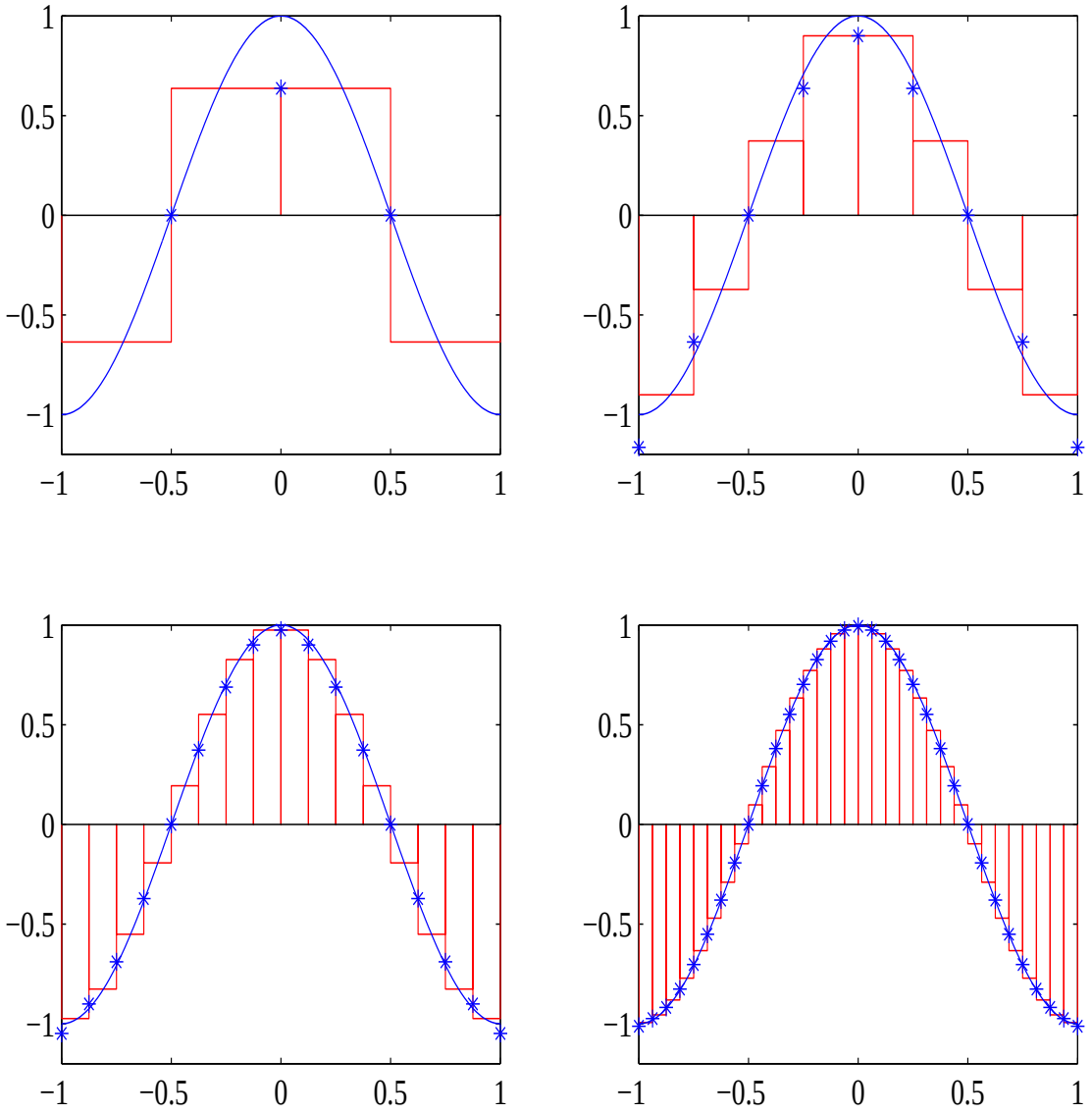

Figure 17.6: Same as figure 17.5 but using piecewise reconstruction interpolation across 2 cells. One-sided reconstruction was used at both end-edges.

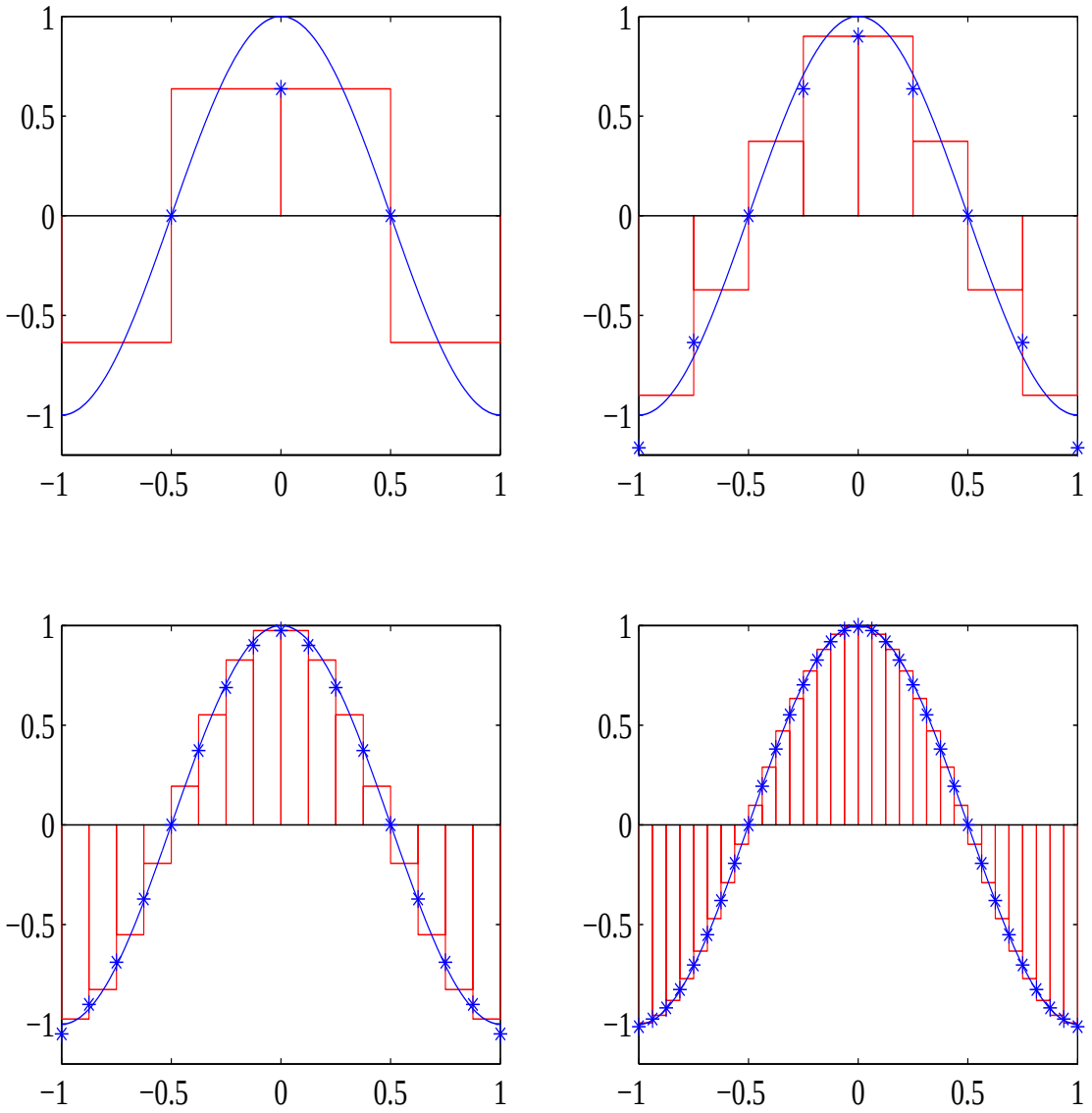

Figure 17.7: Same as figure 17.5 but using piecewise parabolic reconstruction across 3 cells. One sided reconstruction was used for end-edges and for the first internal left edge.

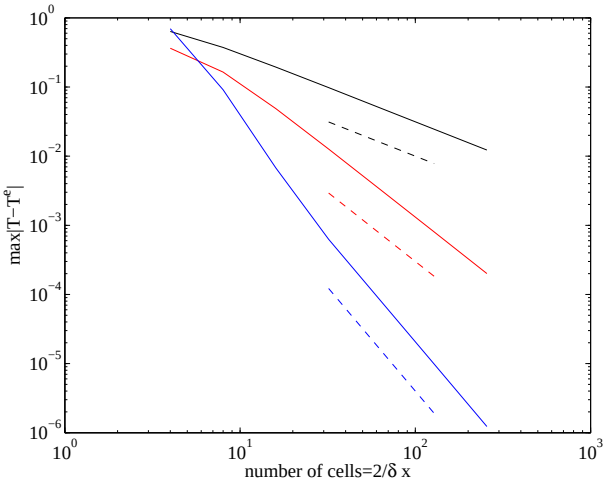

Figure 17.8: Convergence curves showing first, second, and third order convergence for the piecewise constant (black), linear (red) and parabolic (blue) reconstruction procedures, respectively. Reference slopes of N^{-1}, N^{-2} and N^{-3} are shown in dashed line for comparison

.

- The 4 cell discretization is obviously too coarse to represent the cosine wave properly, particularly for the piecewise constant case.
- There is a dramatic improvement in going from to linear to parabolic in the case of the 8 cell discretication (top right panel of figures); whereas the piecewise constant reconstruction still incurs substantial errors.
- The piecewise linear and parabolic reconstruction produce out of bound values (i.e. outside the range of the initial data whose absolute value is bounded by 1) at $x = \pm 1$ because extrapolation had to be used near the edges. This is a recurrent theme in methods whose stencil exceed a single cell.
- The error decreases with increasing cell numbers (decreasing δx) for all three reconstruciton methods considered.
- It is visually apparent that the decrease in error is fastest for the piecewise parabolic reconstruction then for the piecewise constant.

An important issue concerns the rate at which the error decreases for each method. Figure 17.8 shows the convergence curves for the different methods as the number of cells is increased. The slope of the curves on this log-log plot shows the order of the method. For small enough δx, the slope for the constant, linear and parabolic reconstruction asymptotes to -1, -2, and -3 respectively, indicating a convergence of $O(\delta x)$, $O(\delta x^2)$ and $O(\delta x^3)$.

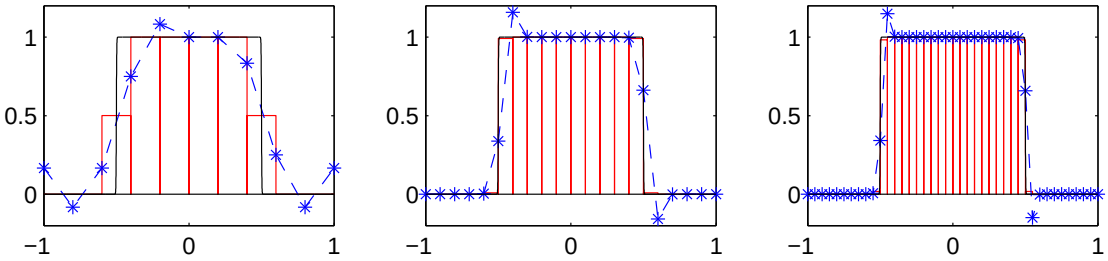

Figure 17.9: Quadratic reconstruction for a function with discontinuity using, from left to right, 10, 20 and 40 cells, respectively, with maximum errors of 0.25, 0.1623, and 0.1580.

17.5 Reconstructing Functions with Discontinuities

The function

$$T(x) = \frac{1}{2}\left(\tanh\frac{x+a}{\delta l} - \tanh\frac{x-a}{\delta l}\right) \tag{17.30}$$

exhibit two transition zones at $x = \pm a$ of width δl as shown in figure 17.5. as δl becomes smaller then the grid spacing, the transition zones appear like discontinuities in the function. High order reconstruction of functions with discontinuities is problematic because of spurious oscillations as shown in figure 17.5 near the discontinuities. The maximum error norm decreases marginally as the number of cell is increased, and does not exhibit the cubic decrease expected for smooth functions. Notice also that the quadratic reconstruction has produced function values outside the range of the original data (larger then 1 at the left discontinuity and a negative value near the right discontinuity). These oscillations are commonly known as Gibbs oscillations and their amplitude does not decrease with increasing resolution. These oscillations are a direct consequence of applying the reconstruction across a stencil that includes a discontinuity. Notice that the first and second order reconstruction cannot produce out of range values, and as such are preferable near sharp transition zones.

Many remedies have been proposed to mitigate the generation of these oscillations. Their common threads is to: first, test for the smoothness of the solution locally, and second, vary the order of the reconstruction and/or the stencil to avoid generating these discontinuities. In sharp transition zone low-order non-oscillatory schemes would be used whereas in smooth regions, high-order reconstruction would be used for improved accuracy. Here we explore one such procedure dubbed the Weighed Essentially Non-Oscillatory scheme (WENO), proposed by Shu and colleagues.

17.5.1 WENO reconstruction

Notice that for the linear reconstruction scheme multiple stencils are available; for example, and assuming the wind to blow from left to right, the following candidate stencils are available to reconstruct the function at $x_{j+\frac{1}{2}}$:

1. S1: T_{j-1}, and T_j
2. S2: T_j and T_{j+1}.

The use of either stencils, S_1 and S_2 would lead to a second-order linear reconstruction. We exclude the stencil $j+1$ and $j+2$ as it would completely violate the characteristic direction. The best 2-point stencil to use for reconstruction is the one with the smoothest variation of the function, a smoothness measure would thus have to be devised.

A second point to notice is that the quadratic reconstruction procedure can be rewritten as a weighed average of the linear reconstruction on stencils S_1 and S_2:

$$T_{j+\frac{1}{2}} = \frac{1}{3}\tilde{T}^{(1)}_{j+\frac{1}{2}} + \frac{2}{3}\tilde{T}^{(2)}_{j+\frac{1}{2}} = \frac{\frac{3\overline{T}_j - \overline{T}_{j-1}}{2} + 2\frac{\overline{T}_j + \overline{T}_{j+1}}{2}}{3} \tag{17.31}$$

where $\tilde{T}^{(s)}_{j+\frac{1}{2}}$ refers to the linear reconstruction on stencil s.

The WENO approach is built upon a similar sort of weighing estimates using weights ω_1 and ω_2 and biasing the weights so that the smoother stencil contributes more then the stencil with rough variations:

$$T_{j+\frac{1}{2}} = \omega_1\tilde{T}^{(1)}_{j+\frac{1}{2}} + \omega_2\tilde{T}^{(2)}_{j+\frac{1}{2}} \tag{17.32}$$

We are now ready to put constraints on our weights:

1. for consistency we require that $\sum_s \omega_s = 1$
2. to guard against worsening oscillations already present in the tilded estimates, we also require that $0 \leq \omega_s \leq 1$.
3. we would like the weights to approach the optimal one: (1/3,2/3) when the two estimates are equally smooth so that we get an improvement in accuracy. This can be acchieved if the weights differ from the optimal weight by an amount of $O(\Delta x)$ for the quadratic case.
4. we would also like the weight to approach zero when the stencil is not not smooth.

Consider the following formula for the weights:

$$\omega_s = \frac{\alpha_s}{\sum_{s=1}^{2}\alpha_s}, \tag{17.33}$$

which trivially satisfies the consistency condition and positivity condition provided $\alpha_s \geq 0$. Furthermore, if we define the α_s as:

$$\alpha_s = \frac{d_s}{(\epsilon + \beta_s)^2} \tag{17.34}$$

where d_s refers to the optimal weight and β_s to the smoothness indicator, then the other conditions would be fullfilled also. Here ϵ is a small positive number included to guard against dividing by zero, and can be taken to be 10^{-7}. The smoothness indicator should be small in smooth stencils and should increase as the variations in the function increase. For the linear reconstruction procedure the smoothness indicator are nothing but the square of the scaled slope across the two cells:

$$\beta_1 = (\overline{T}_j - \overline{T}_{j-1})^2, \quad \beta_2 = (\overline{T}_{j+1} - \overline{T}_j)^2 \tag{17.35}$$

17.5.2 WENO-5

Fifth-order WENO scheme can be devised using simply the three stencils available for the quadratic reconstruction procedure: $S_1 = (j-2, j-1, j)$, $S_2 = (j-1, j, j+1)$, and $S_3 = (j, j+1, j+2)$. These 3 3-point stencils, and the 5-point stencil yield the following estimates for the edge value:

$$\tilde{T}^{(1)}_{j+\frac{1}{2}} = \frac{2\overline{T}_{j-2} - 7\overline{T}_{j-1} + 11\overline{T}_j}{6} \tag{17.36}$$

$$\tilde{T}^{(2)}_{j+\frac{1}{2}} = \frac{-\overline{T}_{j-1} + 5\overline{T}_j + 2\overline{T}_{j+1}}{6} \tag{17.37}$$

$$\tilde{T}^{(3)}_{j+\frac{1}{2}} = \frac{2\overline{T}_j + 5\overline{T}_{j+1} - \overline{T}_{j+2}}{6} \tag{17.38}$$

$$T_{j+\frac{1}{2}} = \frac{2\overline{T}_{j-2} - 13T_{j-1} + 47\overline{T}_j + 27\overline{T}_{j+1} - 3\overline{T}_{j+2}}{60} \tag{17.39}$$

$$T_{j+\frac{1}{2}} = \frac{1}{10}\tilde{T}^{(1)}_{j+\frac{1}{2}} + \frac{6}{10}\tilde{T}^{(2)}_{j+\frac{1}{2}} + \frac{3}{10}\tilde{T}^{(3)}_{j+\frac{1}{2}} \tag{17.40}$$

The optimal weights for the 3 stencils are given by $d_1 = 1/10$, $d_2 = 6/10$ and $d_3 = 3/10$ and yield fifth-order accuracy if used.

The WENO-5 estimate on the other hand is as follows:

$$T_{j+\frac{1}{2}} = \omega_1\tilde{T}^{(1)}_{j+\frac{1}{2}} + \omega_2\tilde{T}^{(2)}_{j+\frac{1}{2}} + \omega_3\tilde{T}^{(3)}_{j+\frac{1}{2}} \tag{17.41}$$

with the weights given by equation 17.34 except that the sum in the denominator runs from over all three stencils. The general formula for the smoothness indicators is

$$\beta_s = \sum_{m=1}^{k} \int_{-\frac{1}{2}}^{\frac{1}{2}} \left(\frac{\partial^m p_s}{\partial x^m}\right)^2 \, \mathrm{d}\xi \tag{17.42}$$

The smoothness indicators include estimate of the slope and curvature now, and are given by:

$$\beta_1 = \frac{13}{12}(\overline{T}_{j-2} - 2\overline{T}_{j-1} + \overline{T}_j)^2 + \frac{1}{4}(\overline{T}_{j-2} - 4\overline{T}_{j-1} + 3\overline{T}_j)^2 \quad (17.43)$$

$$\beta_2 = \frac{13}{12}(\overline{T}_{j-1} - 2\overline{T}_j + \overline{T}_{j+1})^2 + \frac{1}{4}(\overline{T}_{j-1} - \overline{T}_{j+1})^2 \quad (17.44)$$

$$\beta_3 = \frac{13}{12}(\overline{T}_{j+2} - 2\overline{T}_{j+1} + \overline{T}_j)^2 + \frac{1}{4}(\overline{T}_{j+2} - 4\overline{T}_{j+1} + 3\overline{T}_j)^2 \quad (17.45)$$